Scripta Materialia 158 (2019) 46–49

Contents lists available at ScienceDirect

Scripta Materialia

journal homepage: www.elsevier.com/locate/scriptamat

Regular article

Inhomogeneity in thermoelectrics caused by Peltier effect-induced temperature gradient during spark plasma sintering

Yeongseok Kim [a,b], Cheolmin Shin [a], Taesung Kim [a,c,*], Sang-Woo Kang [b,d,**]

[a] School of Mechanical Engineering, Sungkyunkwan University, 2066 Seobu-ro, Jangan-gu, Suwon, Gyeonggi 16419, Republic of Korea
[b] Advanced Instrumentation Institute, Korea Research Institute of Standards and Science, 267 Gajeong-ro, Yuseong-gu, Daejeon 34113, Republic of Korea
[c] SKKU Advanced Institute of Nanotechnology (SAINT), Sungkyunkwan University, 2066 Seobu-ro, Jangan-gu, Suwon, Gyeonggi 16419, Republic of Korea
[d] Science of Measurement, University of Science and Technology, 217 Gajeong-ro, Yuseong-gu, Daejeon 34113, Republic of Korea

ARTICLE INFO

Article history:
Received 20 June 2018
Accepted 14 August 2018
Available online 28 August 2018

Keywords:
Spark plasma sintering
X-ray diffraction (XRD)
Thermoelectric material
Peltier effect

ABSTRACT

This study investigated the reasons for inhomogeneity in the axial direction during spark plasma sintering (SPS) of a thermoelectric material. Bismuth antimony telluride, a p-type thermoelectric material, was sintered using high current (>200 A). X-ray diffraction and power factor analyses confirmed that the preferred orientation improved with increasing sintering temperature, and the power factor increased linearly with temperature. The temperature gradient from 700 to 725 K at 723 K sintering process, estimated from this unique correlation between sintering temperature and power factor, was five-fold that of the reported values. This extraordinary temperature gradient was presumably generated by the Peltier effect.

Spark plasma sintering (SPS) directly heats the target powder as well as the die and punch around it with direct current (DC). As a result, the heat capacity of whole system to be heated, including the material and the SPS equipment, is small, requiring less energy to process than other powder consolidations. In addition, SPS enables rapid sintering and sintering at low temperatures. Moreover, when using a conventional die and punch, it can be applied to various kinds of powder, irrespective of the electrical characteristics of the material [1,2].

Many research groups have studied various SPS process conditions to create high-performance thermoelectric materials [3–5]. Among these process conditions, the sintering temperature has the greatest influence on the properties of the thermoelectric material since it directly affects grain growth [5]. In addition, the thermoelectric power factor tends to be improved by changing the preferred orientation, which depends on the synthesis temperature [5,6].

However, a problem with the SPS process is the non-uniform temperature distribution in the material and SPS tools, such as the die, punch, and foil, during the sintering process. Thus, various simulations to predict this temperature distribution have been reported [7–10]. The temperature gradient that arises during the process produces inhomogeneous materials, thus reducing the yield. Therefore, some studies have attempted to use simulations to reduce the temperature gradient by optimizing the SPS tools [9,10].

However, these models are not suitable for simulating the SPS sintering of a thermoelectric material. These models predict the temperature gradient only considering Joule heating and heat loss. However, in the case of a thermoelectric material, applying DC to the material leads to a Peltier effect, in which additional heat is generated or lost at the opposite ends of the material. Further, this effect can coincide with Joule heating, resulting in a different thermal behavior from that modeled by the conventional simulation [11]. Therefore, experimental studies are required to understand the cause of the inhomogeneity in the SPS process for actual thermoelectric materials.

Therefore, in order to confirm the Peltier effect during the SPS process, we conducted a study to estimate the temperature distribution in the alloy by analyzing the axial inhomogeneity. Using SPS, a typical p-type thermoelectric material, bismuth antimony telluride ($Bi_{0.5}Sb_{1.5}Te_3$, BST), was fabricated from an alloy material. Due to the structure of the SPS equipment, observing the temperature deviation during the sintering process in real time was impossible. Therefore, the sintering temperature and power factor were correlated, and the sintering temperature was estimated using the power factor of the sintered product. In particular, the temperature variation in the upper and lower specimens during the sintering process was estimated by analyzing the sintered alloy in the axial direction. Moreover, compared with that revealed by a previously published numerical analysis results, a significantly larger temperature deviation was observed, which was attributed to the Peltier effect.

* Correspondence to: T. Kim, School of Mechanical Engineering, Sungkyunkwan University, 2066 Seobu-ro, Jangan-gu, Suwon, Gyeonggi 440-746, Republic of Korea.
** Correspondence to: S.-W. Kang, Advanced Instrumentation Institute, Korea Research Institute of Standards and Science, 267 Gajeong-ro, Yuseong-gu, Daejeon 34113, Republic of Korea.
E-mail addresses: tkim@skku.edu (T. Kim), swkang@kriss.re.kr (S.-W. Kang).

https://doi.org/10.1016/j.scriptamat.2018.08.024
1359-6462/

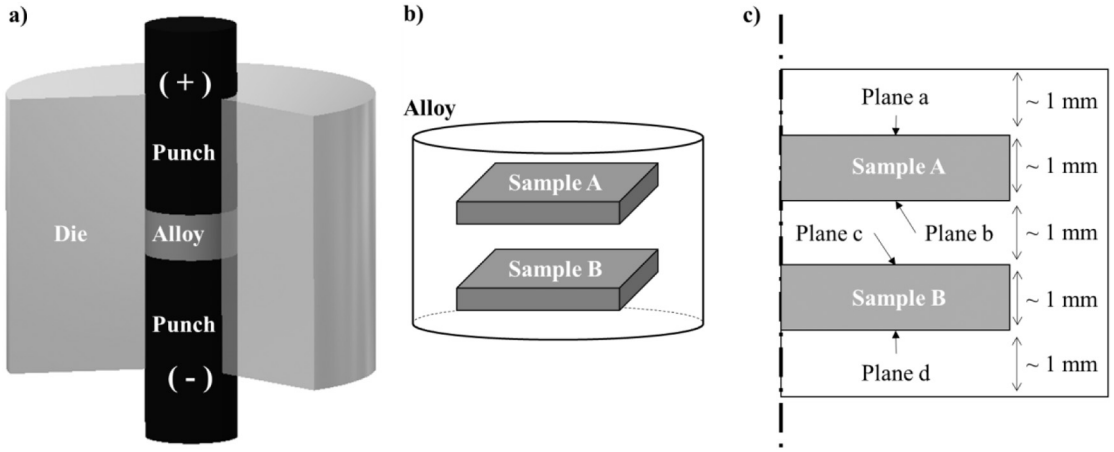

Fig. 1. Experimental and measurement setup. a) Conventional graphite die and punch assembly and its anode and cathode. b) Locations of Samples A and B in the sintered alloy. c) Positions of samples and indices of the Samples and Planes for measurement.

For the experiment, a powder was prepared by using a high-power ball milling machine (SamplePrep 8000D, SPEX) from the commercial BST alloy (Marlow industries). In order to prevent a phase transition in the material during the ball milling process, the duration of ball milling was reduced; six cycles (0.5 h) of ball milling were carried out, each cycle consisting of 5 min of ball milling followed by 10 min of cooling to room temperature(R.T., 296 K). The BMR (ball-to-material ratio) was 1:1 [12].

To prepare the alloy, typical SPS process conditions for BST were used [5], and cold pressing was performed separately to confirm the characteristics of the powder. The sintering equipment was a commercial SPS machine (SPS 211Lx, Fuji) and a conventional graphite SPS tool. (Fig. 1a). The BST alloy was sintered in the shape of a 10 mm (∅) × 5 mm (h) disk using 3 g of BST powder. Five types of alloys were prepared by changing the process temperature to correlate the sintering temperature and power factor. The process conditions of the individual alloys are shown in Table 1.

Two samples of each alloy were fabricated from portions at opposite ends of the sintered alloy, as shown in Fig. 1b, which demonstrates the positions of each prepared sample. The upper and lower parts of the sintered specimen were ground down by about 1 mm to eliminate the edge regions where carbon uptake occurred, which is characteristic of the SPS process [13]. Then, the sample was fabricated by processing the positive electrode tip into a plate with dimension of 7.5 mm (w) × 3.5 mm (l) × 1 mm (t).

The fabricated samples were analyzed using energy dispersive X-ray spectroscopy (EDS, S4800, Hitachi), X-ray diffraction, (XRD, SmartLab, Rigaku) and the power factor (LSR-3, Linseis). In order to confirm the stability of the sintering process, the composition ratio was confirmed by EDS, and the XRD peak pattern was analyzed. Then, the power factor in the in-plane direction was measured at various positions in the z-direction, and the results were compared with the degree of orientation, which were calculated based on the XRD peak intensity [5,6]. The alloy samples and planes are classified in Table 1 according to the process conditions and positions.

First, to analyze the correlation between the sintering temperature and power factor, Plane c of Sample B, which corresponds to the center of the alloy, was analyzed depending on sintering temperature. As revealed by the EDS quantitative analysis in Fig. 2a and the XRD patterns in Fig. 2b, the composition and crystal phase do not greatly vary under the sintering conditions used in this process; thus, the BST alloy can be stably manufactured. In addition, as shown in Fig. 2b, only the sharpness of the peaks differs from that of the cold-pressed SPS material. This suggests that although the crystal phase of the powder is mainly present, fine grain growth and reorientation occur during the sintering process, resulting in a small amount of other phases.

On the other hand, Fig. 2c shows a linear correlation between the sample temperature and the power factor for various sintering temperatures and the cold-pressed materials without powder consolidation. In particular, Fig. 2d shows the maximum power factor as a function of sintering temperature. Clearly, the sintering temperature strongly correlates with the power factor. This is because as the sintering temperature increases, the specific gravity of the (0 0 *l*) orientation increases, resulting in improved carrier transport in the in-plane direction of the BST [5,6]. The increase in the proportion of the (0 0 l) orientation is also confirmed by the increasing degree of orientation in Fig. 2e, calculated from the XRD results [5].

Therefore, the temperature distribution of the sintered alloy was estimated using the correlation between the power factor and the sintering temperature (Fig. 3a). The highest temperature deviation occurs in the upper and lower parts of the alloy, and this deviation can reach up to 30 K. In addition, the temperature difference between the

Table 1
Index of sample and plane depending on the SPS process condition.

Index	Technique	Sintering temperature [K]	Holding time [min]	Uniaxial pressure [MPa]	Ramp rate [K/min]	Sample (EDS, XRD)	Plane (Power factor)
CP-B	Cold press	296 (R.T.)	540	50	–	B	c
S-623-B	SPS	623	5	50	85	B	c
S-673-B		673	5	50	85	B	c
S-723-A-a		723	5	50	85	A	a
S-723-A-b							b
S-723-B-c						B	c
S-723-B-d							d
S-773-B		773	5	50	85	B	c